An analytical model to simulate tension stiffening mechanism in moment-rotation response of FRC flexural members with tensile longitudinal reinforcement

Mahsa Taheri

PhD Student, ISISE, , Dep. Civil Eng., School Eng., University of Minho

taheri@civil.uminho.pt

Joaquim A. O. Barros

Full Professor, ISISE, Dep. Civil Eng., School Eng., University of Minho

barros@civil.uminho.pt

Report 12-DEC/E-24

Date: September 2012

Pages: 36

School of Engineering | Department of Civil Engineering | University of Minho | Fundação para a Ciência e Tecnologia

TABLE OF CONTENTS

1 INTRODUCTION

Taking advantage of steel reinforcement in order to increase the tensile load carrying capacity of concrete is traditional approach in reinforced concrete (RC) elements to overcome the inherent weakness of concrete in tension. Nevertheless even by the use of enough tensile reinforcement, the early stage cracking of concrete cover due to shrinkage or preliminary loading, formation of cracks cannot be completely overcome. Corrosive agents may penetrate among these cracks and affect negatively load carrying capacity of RC members by decreasing the effective area of steel reinforcement and reduction of interaction between steel and concrete.

Substitution of steel bars by fibre reinforced polymer (FRP) composite materials, with higher resistance against adverse environmental conditions, has been an effort to reach more durable reinforced concrete structures. However, experimental studies revealed that the total replacement of steel by FRP is not justifiable due to the initial higher costs of some high stiff reinforcement systems (like those based on the use of carbon fibres – CFRP) or relatively low elasticity modulus of more cost-justifiable systems like those made by glass fibres (GFRP). In any case the FRP systems present an elastic-brittle failure mode, which can be quite concerning in terms of assuring a ductile behaviour for a concrete structure.

Taking the benefits that can be obtained by adding discrete fibres to cement based composits, fibre reinforced concrete (FRC) materials can be produced with relatively high post-cracking residual strength, capable of eliminating conventional steel reinforcement elements, mainly those more susceptible to corrosion, such is the case of steel stirrups, especially when applied in beams of relatively thin web.

The use of FRC of different post-cracking behaviour, presenting tensile strain softening or tensile strain hardening [1], for beams strengthened with steel and FRP bars, was already investigated by Author through developing an analytically model capable of determining the moment-curvature relationship $(M-\chi)$ of a rectangular cross section of this type of beams, failing in bending [2]. A parametric study with this model was then carried out to investigate the influence of the characteristics of the FRC for the flexural reinforcement of RC beams failing in bending [3]. Finally the model was extended in order to explore the potentialities of using prestressed FRP and steel bars for the flexural reinforcement of FRC beams [4].

The moment-curvature $(M-\chi)$ approach is based on Bernoulli's linear strain profiles (Fig. 1a). For the case of reinforced concrete members, linearity of strain profile necessitates considering an

equal strain for both reinforcement and its surrounding concrete. This means to adopt the moment-curvature method for RC members, a full-interaction (perfect bond) between concrete and reinforcement should be assumed, which can be a too rudimental assumption, mainly if crack width, deflection and load carrying capacity for service limit states needs to be accurately predicted. Furthermore, the contribution of the post-cracking residual strength is modelled by a stress-strain approach, which poses difficulties on bridging the stress-crack width relationship derived from experimental tests executed to assess the tensile performance of FRC, and the stress-strain approach adopted by designers.

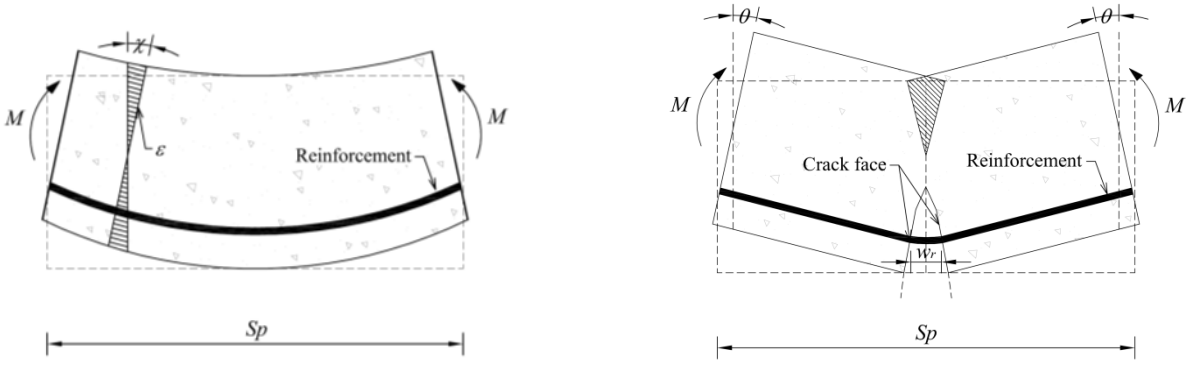

(a) (b)

Fig. 1: Flexural deformation of reinforced concrete element according to (a) Moment-curvature and (b) Moment-rotation approach

In a cracked RC flexural element, simultaneous with crack widening, a rigid body rotation occurs on two half of intact part joined together (Fig. 1b). Internal moment of the cracked section in each step of loading can be correlated to the rotation of section (θ) with so-called moment rotation approach. In the present report, taking advantage of concept of moment-rotation $(M-\theta)$ an analytical procedure is developed to determine the load carrying capacity of flexural FRC elements strengthened by tensile longitudinal reinforcement. The model is capable to simulate the debonding between reinforcement and the surrounding concrete, the crack propagation with a stress-crack width law, and the shear friction mechanism of concrete in compression. To develop the aimed model, collaboration of concrete and reinforcement in load bearing procedure are distinctly simulated, and then will be mobilized in a final analytical model.

2 COLLABORATION OF COMPRESSIVE CONCRETE IN LOAD CARRYING MECHANISM

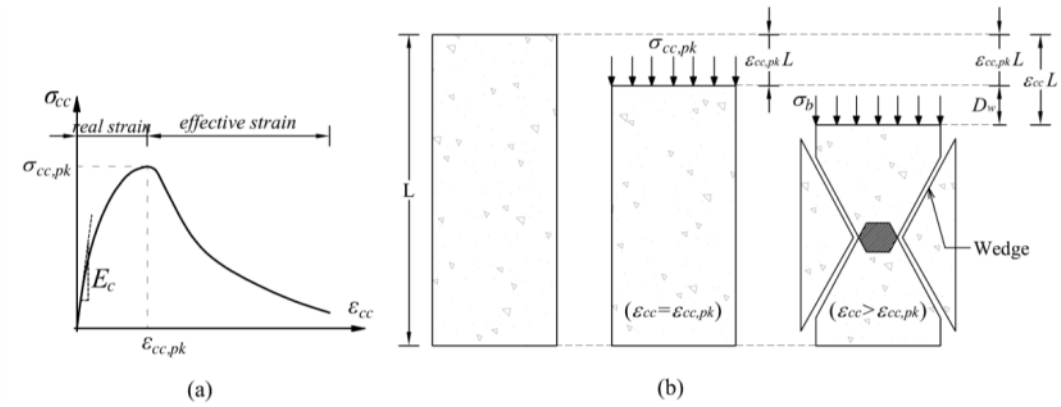

Fig. 2: (a) Compressive stress-strain relationship of concrete, (b) wedge sliding mechanism in uniaxial compression (adapted from [5])

A typical compressive stress-strain of concrete is depicted in Fig. 2a where the initial ascending branch is followed by a softening curve beyond peak point. The pre-peak part of the curve is related to material property of concrete can be represented by taking advantage of a models proposed in literatures. Here assuming Hognestad's parabolic stress distribution [6], the compressive stress of concrete can be obtained from Eq. 1:

$$\sigma_{cc} = \sigma_{cc,pk}\left(\frac{2\varepsilon_{cc}}{\varepsilon_{cc,pk}} - \left(\frac{\varepsilon_{cc}}{\varepsilon_{cc,pk}}\right)^2\right) \tag{1}$$

where $\sigma_{cc,pk}$ represents the compressive strength of concrete and its corresponding strain $\left(\varepsilon_{cc,pk}\right)$ can be determined from equation below [7]:

$$\varepsilon_{cc,pk} = (-0.067\,\sigma_{cc,pk} + 29.9\,\sigma_{cc,pk} + 1053)\times 10^{-6} \tag{2}$$

Once the peak stress $\sigma_{cc,pk}$ is achieved, wedge sliding mechanism forms in compressive element. The deterioration of compressive stress-strain in softening branch is a consequence of reduction of the internal forces transferring across the sliding planes [8,9] (Fig. 2b).

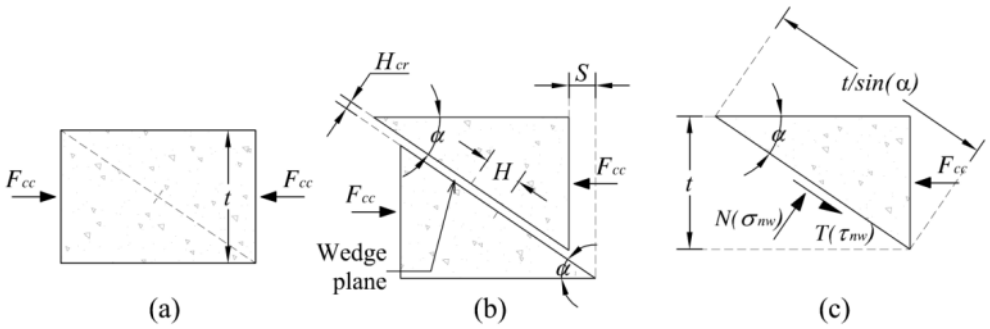

Fig. 3: Wedge sliding mechanism (a) concrete element under lateral pressure; (b) wedged element displacement; (c) wedged element forces

The wedge sliding mechanism is dependent on the shear friction characteristics of concrete [9,10]. In Fig. 3a a concrete element with a thickness of t, subjected to lateral compressive force of F_{cc}. The wedge sliding displacements and force components are depicted in Fig. 3b and 3c, respectively. Assuming wedge angel of α, the tangential displacement of wedge (H) can be resulted from the wedge displacement aligned with applied pressure (S):

$$H = \frac{S}{\cos\alpha} + H_{cr} \tan\alpha \tag{3}$$

where H_{cr} is the displacement normal to the sliding planes. Magnitude of H_{cr} is so smaller than S, so neglecting the second part of the above equation, we can have:

$$H = \frac{S}{\cos\alpha} \tag{4}$$

The angle of the wedge α in the above equations depends on the Mohr-Coulomb frictional property of concrete and can be assumed 37° for ordinary concrete. T and N In Fig. 3c are, respectively, the force components tangential and normal to the wedge plane can be obtained from τ_{nw} and σ_{nw}, shear stress and normal stress of concrete in wedge plane. τ_{nw} and σ_{nw} can be correlated together with H, by Eq. 5 [10]:

$$\tau_{nw} = \left[\left(-30.142 + 51.623\frac{\sigma_{nw}}{\sigma_{cc,pk}}\right)H\right]\left(\frac{\sigma_{cc,pk}}{30}\right)^{0.91} + 0.497\sigma_{cc,pk} \qquad (N \text{ and } mm) \tag{5}$$

According to Fig. 3c, the force components of wedge plane are determined as:

$$T = \frac{\tau_{nw} t b}{\sin \alpha} \tag{6}$$

$$N = \frac{\sigma_{nw} t b}{\sin \alpha} \tag{7}$$

where b and t are, respectively, the width and thickness of loaded face of the element. Satisfying force equilibrium in Fig. 3c in vertical direction gives:

$$N = T \tan \alpha \tag{8}$$

And consequently:

$$\sigma_{nw} = \tau_{nw} \tan \alpha \tag{9}$$

Simultaneously solving Eq. 5 in Eq. 9, τ_{nw} and σ_{nw} will be obtained for a known value of H. Satisfying force equilibrium in Fig. 3c in horizontal direction, the compressive force applied on the element is obtained:

$$F_{cc} = T \cos \alpha + N \sin \alpha \tag{10}$$

In a flexural reinforced concrete element, when enough strong reinforcing scheme be adopted in tensile region, simultaneous with crack widening in tensile zone, concrete stress in compressive region may tend to compressive strength of concrete and consequently, as explained earlier the wedge sliding mechanism [11] may be forms as depicted by hatched area in Fig. 4.

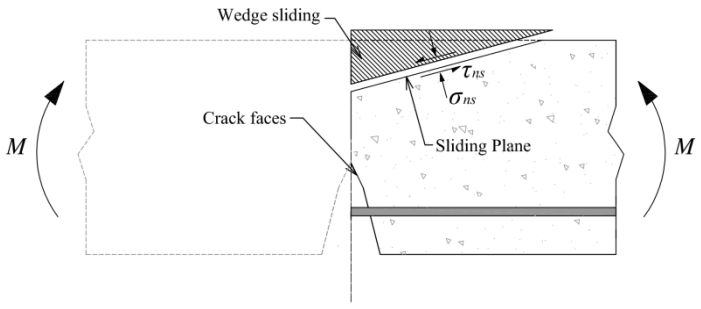

Fig. 4: Sliding wedge mechanism (interior-intact) in flexural reinforced element (adapted from [12])

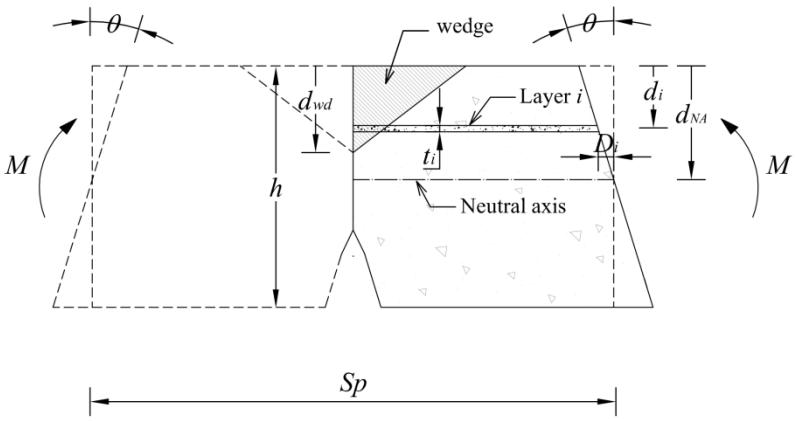

Fig. 5: Deformation of compressive region of flexural concrete element

To take into account the compressive property of concrete in the aimed model, a segment of the beam with a length of S_p imposed by a certain rotation of θ is considered according to Fig. 5, where height of the wedge is designated by d_{wd} . The deformation of ith layer, located in the compressive region (upper than neutral axis) with a depth of d_i can be obtained from Eq. 11:

$$D_i = \theta(d_{NA} - d_i) \tag{11}$$

For the layers located outside the wedge region $(d_{wd} < d_i)$ compressive stress of concrete is in ascending branch of stress-strain diagram (Fig. 2a) and the corresponding deflection is based on material properties of concrete. Hence for these layers the compressive strain can be obtained directly from the deflection:

$$\varepsilon_{cc,i} = 2D_i / S_p \quad (d_{wd} < d_i < d_{NA}) \tag{12}$$

Substituting $\varepsilon_{cc,i}$ in Eq. 1, the compressive stress of layer $i\left(\sigma_{cc,i}\right)$ is achieved, by which compressive force of layer i is determined from equation below:

$$F_{cc,i} = b_i t_i \sigma_{cc,i} \quad (d_{wd} < d_i < d_{NA}) \tag{13}$$

where t_i and b_i are the thickness and width of layer i, respectively. However as explained earlier the compressive deformation of D_i obtained for the layers located inside the wedge $(d_i < d_{wd})$ includes both material contraction and component of wedge sliding mechanism:

$$D_i = \varepsilon_i S_p / 2 + S_i \quad (d_i < d_{wd}) \tag{14}$$

Values of S_i and ε_i in above equation can be obtained from an iterative procedure, in which an imaginary value is first assigned to ε_i, designated by ε_i', and corresponding sliding deformation $\left(S_i'\right)$ of the layer is obtained:

$$S_i' = D_i - \varepsilon_i' S_p / 2 \tag{15}$$

Taking advantage of Eq. 4, the tangential sliding of the layer (H) is determined and used in Eq. 5. Substituting σ_{nw} in Eq. 6 by Eq. 9, τ_{nw} will be obtained from Eq. 5, according which by going back to Eq. 9, σ_{nw} is then be determined. Substituting values of σ_{nw} and τ_{nw} in Eq. 6 and 7, T and N are obtained. These two force components should be finally utilized in Eq. 10, to determine the compressive force of layer $i\left(F_{cc,i}\right)$, according which, the compressive stress of the layer can be obtained from Eq. 16:

$$\sigma_{cc,i}' = \frac{F_{cc,i}}{b_i t_i} \tag{16}$$

Substituting $\sigma_{cc,i}'$ in Eq. 1, corresponding compressive strain of the layer $\varepsilon_{cc,i}'$ is determined inversely, should be equal to the initial guess $\left(\varepsilon_i'\right)$, otherwise aforementioned procedure will be followed again with a new ε_i'.

3 COLLABORATION OF TENSILE FRC IN LOAD CARRYING MECHANISM

Contrary to plain concrete, FRC materials capable of forming multi cracks in tension, which leads to a significant increase in energy absorption capacity and a pseudo-ductile behaviour, due to the fibre pullout mechanisms that limit the crack propagation [13]. The use of FRC in structural applications is an effective approach to overcome the tension weakness of concrete and mitigate the structural deteriorations due to corrosion of steel reinforcement [14]. Depending on the mix design, volume content and geometry of fibres, FRCs are able to represent different levels of post-cracking response in tension as depicted in Fig. 6. The strain softening behaviour (SS), characterized by a decrease of tensile stress with the increase of tensile deformation after cracking stress, while the

tensile strain hardening (SH) FRCs are identified by tensile strength much higher than cracking stress with large strain up to failure [15-17]. Beyond tensile strength, SS- and SH-FRC materials represent a softening deterioration up to failure due to localization of dominant crack. Therefore in order to characterize FRC in tension, the stress-strain relationship $(\sigma_{ct} - \varepsilon_{ct})$ of FRC is utilized before tensile strength attained. Then the tensile stress-crack width relationship $(\sigma_{ct} - w)$ will be used.

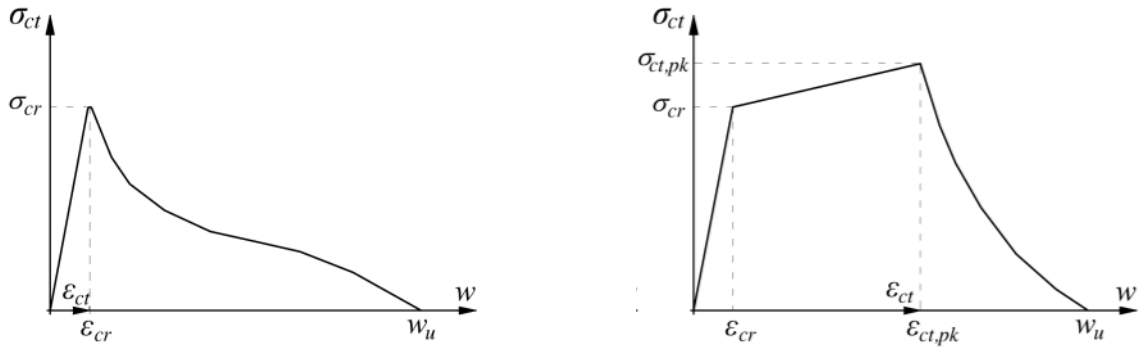

(a) (b)

Fig. 6: Typical stress-strain and stress-crack width of ; (a) strain softening and; (b) strain hardening FRC in tension.

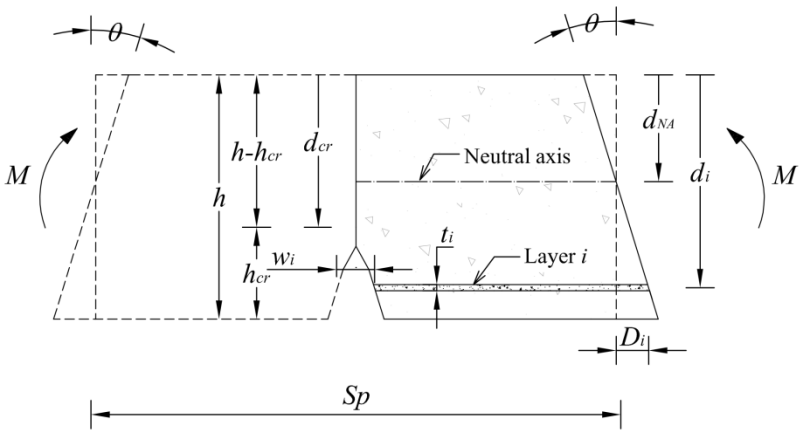

Fig. 7: Simplified deformation of concrete in tension region of cracked section

In Fig. 7 is depicted a FRC prism with a length of S_P imposed by a certain rotation of θ, where the depth of crack tip is designated by d_{cr}. The deformation of ith layer, located at depth of d_i in tensile region can be obtained from Eq. 17:

$$D_i = \theta(d_i - d_{NA}) \tag{17}$$

Deformation of the layers positioned upper than the crack tip in tensile region $\left(d_{NA} < d_i < d_{cr}\right)$ is due to the material property of intact concrete. So the tensile strain of the layers $\left(\varepsilon_{ct,i}\right)$ and corresponding stress $\left(\sigma_{ct,i}\right)$ can be obtained from the following equations:

$$\varepsilon_{ct,i} = 2D_i / S_p \tag{18}$$

$$\sigma_{ct,i} = \sigma_{ct}\left(\varepsilon_{ct,i}\right) \quad \left(\text{for } d_{NA} < d_i < d_{cr}\right) \tag{19}$$

For the layers located in cracked region $\left(d_{cr} < d_i\right)$, the width of crack at layer's level can be obtained from equation below:

$$w_i = \left[2D_i - \frac{\sigma_{ct}\left(w_i\right)}{E_c} S_p\right] \tag{20}$$

The tensile stress of the layer can be obtained :

$$\sigma_{ct,i} = \sigma_{ct}\left(w_i\right) \quad \left(\text{for } d_{cr} < d_i\right) \tag{21}$$

The resultant tensile force of layer i can be finally obtained from Eq. 22, in which t_i and b_i are the thickness and width of ith layer, respectively.

$$F_{ct,i} = \sigma_{ct,i} b_i t_i \tag{22}$$

4 BOND-SLIP RESPONSE BETWEEN REINFORCEMENT AND FIBROUS CONCRETE

Crack width and crack spacing, deflections, structural strength, and energy absorption and dissipation capacities of reinforced concrete members are all related directly or indirectly to the bond characterization of interface between concrete and reinforcement.

Confinement of concrete is one of the most practical and effective procedure to improve the bond-slip behaviours. According to the experimental evidence, discrete fibres distributed in concrete, due to their restraining to the opening of micro cracks, can confer certain levels of confinement to the concrete surrounding the reinforcement and, consequently, they improve the bond behaviour [18]. The effect of steel fibres on the improvement of the ductility of bond failure was revealed in [19]. Harajli et al. [20] studied the effects of steel fibres on bond behaviour of steel reinforced FRC, by

defining the index of fibre reinforcing $\left(V_f L_f / d_f\right)$, according which an increment from 26 to 33% of the local bond strength, with respect to the samples made by plain concrete, were observed by increasing the volume fraction of fibres from 1 and 2%. Efficiency of fibre content to enhance the bound behaviour was also investigated in [21] on specimens made by SFRC and reinforced simultaneously by longitudinal steel bar and transversal steel stirrups. The test results revealed that by increasing the volume content of fibres from 0.5% to 1.0% had a negligible effect on ultimate bond strength, due to much higher level of confinement provided by the stirrups.

Due to different mechanical and physical properties of FRP surface, the bond mechanism in FRP bars embedded in concrete differs from steel bars [22]. In spite of a numerous studies conducted on bond characteristics between FRP bars and concrete [23-29], there is still a lack of reliable local bond equations between these materials. The bond characteristics of FRP bars and fibrous concrete are not proposed in Model code [30]. Mazaheripour et al. [31] studied the bond behaviour of GFRP bars surrounded by self compacting fibre reinforced concrete (SFRSCC) with 0.8% volume fraction of hook ends steel fibres. They observed the bond strength is decreased by increasing of bond length. The improvement of bond behaviours by decreasing the reinforcing bars diameter was concluded in [26, 32]. In an experimental research carried out by Belarbi and Wang [33], the bond behaviour between polypropylene fibre reinforced concrete (PFRC) and GFRP and CFRP bars were investigated. Surface of the GFRP bars was wrapped with helical fibre strand, while CFRP bars had a very smooth surface. According to the test observations these authors concluded that the rough surface of GFRP bars had a significant effect on improving the bond strength since it was twice larger than the bond strength obtained in CFRP bars. The efficiency of polypropylene fibres as discrete reinforcement of concrete seems much higher for the bond ductility than for the bond strength. The average bond strength of GFRP bars was decreased by increasing the bond length as observed in [31], while the opposite impact was obtained for CFRP reinforcement.

in Fig. 8, are depicted some idealized bond-slip characteristic between concrete and reinforcing bars, where the peak shear stress τ_f occurs at a slip δ_1; and δ_f is the peak slip beyond which the shear stress can be assumed to be zero.

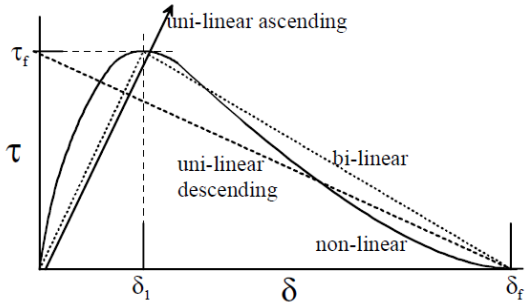

Fig. 8: Typical bond-slip relationship of interface of concrete and reinforcement

5 IMPACT OF BOND ON COLLABORATION OF TENSILE REINFORCEMENT IN LOAD CARRYING MECHANISM

Fig. 9a shows a reinforced concrete element subjected to the direct pull test. A prism of element around a formed crack is parted in Fig. 9b and cross section of element is depicted in Fig. 9c.

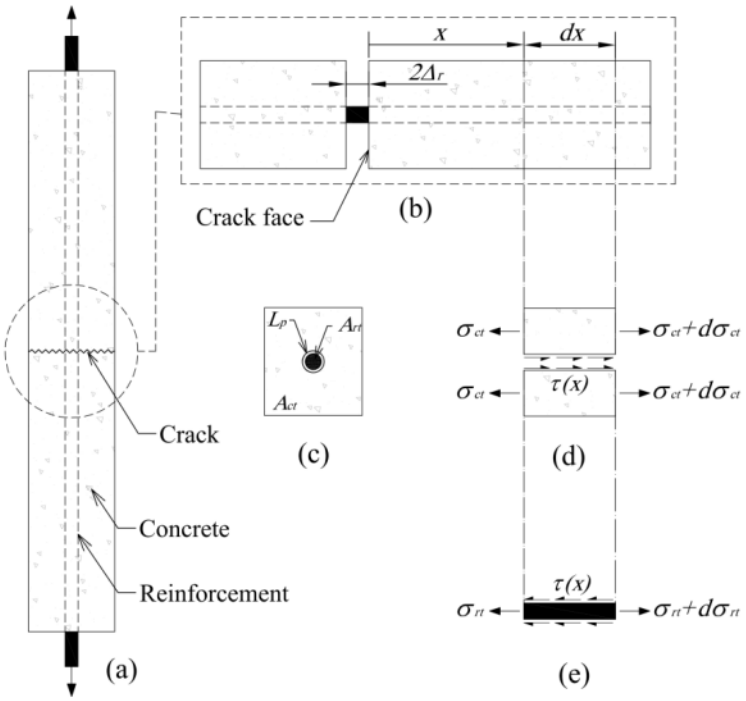

Fig. 9: Shear bond and tensile stress distribution in reinforced concrete under uniaxial tension

Equilibrium between of tensile stress of concrete (σ_{ct}) and reinforcement (σ_{rt}), and shear bond stress interface (τ) for a length of dx can be represented as (Fig. 9d and 9e):

$$\left(\sigma_{ct}(x)+d\sigma_{ct}\right)A_c-\sigma_{ct}(x)A_c-\tau(x)L_p dx=0 \tag{23}$$

$$\left(\sigma_{rt}(x)+d\sigma_{rt}(x)\right)A_r-\sigma_{rt}(x)A_r+\tau(x)L_p dx=0 \tag{24}$$

where A_r, A_c are the area of reinforcement and surrounding concrete, respectively, and L_p is the circumference of the reinforcement. Eqs. 23 and 24 can be reduced to:

$$\frac{d\sigma_{ct}(x)}{dx}=\frac{\tau(x)L_p}{A_c} \tag{25}$$

$$\frac{d\sigma_{rt}(x)}{dx}=-\frac{\tau(x)L_p}{A_r} \tag{26}$$

The slip of interface along interaction $\left(\delta(x)\right)$ can be assumed as a difference between axial displacement of the surrounding concrete $\left(u_c(x)\right)$ and reinforcement $\left(u_r(x)\right)$:

$$\delta(x)=u_c(x)-u_r(x) \tag{27}$$

Differentiating two sides of the above equation gives:

$$\frac{d\delta(x)}{dx}=\frac{du_c(x)}{dx}-\frac{du_r(x)}{dx} \tag{28}$$

$\frac{du_c(x)}{dx}$ and $\frac{du_r(x)}{dx}$ in above equations represent the tensile strain of concrete and reinforcement, respectively, can be obtained from:

$$\frac{du_c(x)}{dx}=\frac{\sigma_c(x)}{E_c} \tag{29}$$

$$\frac{du_r(x)}{dx}=\frac{\sigma_r(x)}{E_r} \tag{30}$$

where a linear stress-strain response with elastic modulus of E_c and E_r is utilized for concrete and reinforcement, respectively. Substituting Eqs. 29 and 30 in Eq. 28 and differentiating give the fallowing equations:

$$\frac{d\delta(x)}{dx} = \frac{\sigma_c(x)}{E_c} - \frac{\sigma_r(x)}{E_r} \tag{31}$$

$$\frac{d^2\delta(x)}{dx^2} = \frac{1}{E_c}\left(\frac{d\sigma_c(x)}{dx}\right) - \frac{1}{E_r}\left(\frac{d\sigma_r(x)}{dx}\right) \tag{32}$$

Finally, substituting Eqs. 25 and 26 in Eq. 32 gives a differential equation represents correlation between shear bond and slip displacement of interface along interaction (x):

$$\frac{d^2\delta(x)}{dx^2} - \beta_2\tau(x) = 0 \tag{33}$$

where:

$$\beta_2 = \frac{L_p}{A_r}\left(\frac{A_r}{E_c A_c} + \frac{1}{E_r}\right) \tag{34}$$

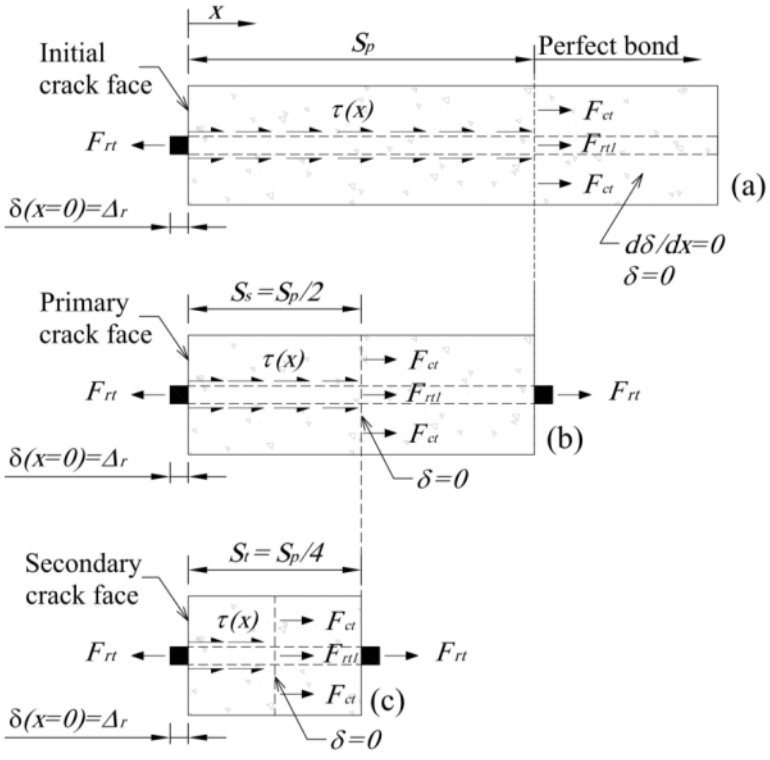

Fig. 10: Tension stiffening mechanism in a reinforced concrete prism

The boundary conditions required to resolve the differential equation of 33, can be obtained taking advantage of tension stiffening mechanism as depicted typically in Fig. 10 for a prism of reinforced concrete adjacent to a formed initial crack (at $x = 0$). At initial crack, , the slip strain is the difference

between the strain in the surrounding concrete and in the reinforcement can be resulted from Eq. 31 as:

$$\frac{d\delta(x=0)}{dx} = \frac{\sigma_c(x=0)}{E_c} - \frac{\sigma_r(x=0)}{E_r} \tag{35}$$

can be rewritten as:

$$\frac{d\delta(x=0)}{dx} = \frac{\sigma_{ct}(w_i)}{E_c} - \frac{F_{rt}}{A_r E_r} \tag{36}$$

At this point, the slip is assumed equal to elongation of the reinforcement (Δ_r):

$$\delta(x=0) = \Delta_r \tag{37}$$

It is assumed the primary crack will be formed by a minimum distance of S_p with respect to the initial crack face, as depicted in Fig. 10a, where both slip strain and slip tend toward zero:

$$\frac{d\delta(x=S_p)}{dx} = 0 \tag{38}$$

$$\delta(x=S_p) = 0 \tag{39}$$

Beyond S_p full interaction region can be assumed for the interface. The distribution of internal stresses just after formation of primary crack is depicted in Fig. 10b, according which, the intact concrete between initial and primary cracks is considered as a symmetrically loaded prism of length S_p. So the next crack, designated by secondary crack, is expected to be formed at middle of the prism ($S_s = \frac{S_p}{2}$). Considering the symmetrically loading, boundary conditions just before secondary crack are represented in the equations below:

$$\frac{d\delta(x=S_p/2)}{dx} \neq 0 \tag{40}$$

$$\delta(x=S_p/2) = 0 \tag{41}$$

If the bond is sufficiently strong, tertiary crack may form at the midpoint of the prism of length S_s (Fig. 10c) at which the boundary conditions are:

$$\frac{d\delta\left(x = S_p / 4\right)}{dx} \neq 0 \tag{42}$$

$$\delta\left(x = S_p / 4\right) = 0 \tag{43}$$

Here, In a simple way, a linear ascending relationship is considered between bond stress and slip deformation of concrete and reinforcement interface, represented by Eq. 46

$$\tau = k_e \delta \tag{44}$$

where k_e is the stiffness of the bond-slip. Substituting the above definition of bond stress in Eq. 33, the differential gives:

$$\frac{d^2\delta(x)}{dx^2} - \beta_2 k_e \delta(x) = 0 \tag{45}$$

The homogeneous solution of above differential equation can be represented as below:

$$\delta(x) = a\cosh(\lambda_1 x) + b\sinh(\lambda_1 x) \tag{46}$$

And when differentiated:

$$\frac{d\delta(x)}{dx} = \lambda_1 a\sinh(\lambda_1 x) + \lambda_1 b\cosh(\lambda_1 x) \tag{47}$$

where:

$$\lambda_1 = \sqrt{k_e \beta_2} \tag{48}$$

Substituting Eq. 46 into Eq. 44, variation of bond stress along the interaction length is obtained:

$$\tau(x) = k_e\left[a\cosh(\lambda_1 x) + b\sinh(\lambda_1 x)\right] \tag{49}$$

a and *b* parameters in above equations are constant values determined according to the boundary conditions explained earlier. Adopting the condition represented in Eq. 36 gives:

$$b = -\frac{1}{\lambda_1}\left(\frac{F_{rt}}{A_r E_r} - \frac{\sigma_{ct}(w_i)}{E_c}\right) \tag{50}$$

Satisfying the conditions of Eqs. 38 and 39, the following equations are obtained:

$$\lambda_1 a \sinh(\lambda_1 S_p) + \lambda_1 b \cosh(\lambda_1 S_p) = 0 \quad (51)$$

$$a \cosh(\lambda_1 S_p) + b \sinh(\lambda_1 S_p) = 0 \quad (52)$$

In the above hyperbolic equations, *a* parameter and S_p are unknown. From Eq. 52:

$$a = -b \tanh(\lambda_1 S_p) \quad (53)$$

By substituting of Eq. 53 in Eq. 51 the primary crack spacing will be equal to :

$$S_p = \frac{2}{\lambda_1} \quad (54)$$

Substituting S_p obtained from the above equation in to Eq. 53 yields:

$$a = -b \tanh(2) \quad (55)$$

According to Fig. 10a internal force of reinforcement at initial crack (F_{rt}) can be correlated to the internal force of reinforcement (F_{rt1}) and surrounding concrete (F_{ct}) at primary crack as:

$$F_{rt} = F_{rt1} + F_{ct} \quad (56)$$

According to Fig 10a it can also be written:

$$F_{rt} - \int_{x=0}^{x=S_p} \tau(x) L_p dx = F_{rt1} \quad (57)$$

Merging Eqs. 56 and 57, the maximum bond force developed between reinforcement and concrete can be determined from the following equation:

$$\int_{x=0}^{x=S_p} \tau(x) L_p dx = f_{ct} A_c \quad (58)$$

where f_{ct} is the tensile cracking stress of concrete. Since the full interaction condition is assumed beyond S_p, the strain of reinforcement and concrete are equal, so it can be written:

$$F_{rt1} = \frac{\sigma_c}{E_c} A_r E_r \tag{59}$$

Substituting Eqs. 58 and 59 into Eq. 57 the internal force of reinforcement, corresponding to formation of primary crack is determined:

$$F_{rt,cr} = \frac{f_{ct}}{E_c} A_r E_r + f_{ct} A_c \tag{60}$$

For the assumed linear ascending bond-slip relationship, substituting Eqs. 58 and 59 into Eq. 57 gives the load corresponding to the formation of primary crack:

$$F_{rt,cr}^{pr} = \frac{(0.72 k_e L_p \sigma_{ct}(w_i) + \lambda_1^2 \varepsilon_{cr} E_c^2 A_c) A_r E_r}{0.72 k_e L_p E_c} \tag{61}$$

Adopting boundary condition of Eq. 41, a parameter is obtained corresponding to formation of secondary crack:

$$a = -b \tanh(1) \tag{62}$$

Substituting Eqs. 62 and Eq. 50 into Eq. 46 and again into Eq. 49, gives the load corresponding to formation of secondary crack as:

$$F_{rt,cr}^{\sec} = \frac{(0.35 k_e L_p \sigma_{ct}(w_i) + \lambda_1^2 \varepsilon_{cr} E_c^2 A_c) A_r E_r}{0.35 k_e L_p E_c} \tag{63}$$

Similarly, a parameter and internal force of reinforcement corresponding to the formation to tertiary crack, is determined from the following equations:

$$a = -b \tanh(0.5) \tag{64}$$

$$F_{rt,cr}^{ter} = \frac{(0.11 k_e L_p \sigma_{ct}(w_i) + \lambda_1^2 \varepsilon_{cr} E_c^2 A_c) A_r E_r}{0.11 k_e L_p E_c} \tag{65}$$

In Fig. 11 is simplified deformation of a flexural concrete element reinforced longitudinally in tension surrounded by concrete cover of c . The tensile load transferred by the reinforcement is influenced by the interaction characteristics between reinforcement and surrounding concrete. Here, in order to simplicity, association of reinforcement in load bearing mechanism is considered in two

distinct phases. In the first phase, depicted in Fig. 11a, the formed flexural crack does not cross the reinforcement $(d_r < d_{cr})$, for which a full interaction is assumed.

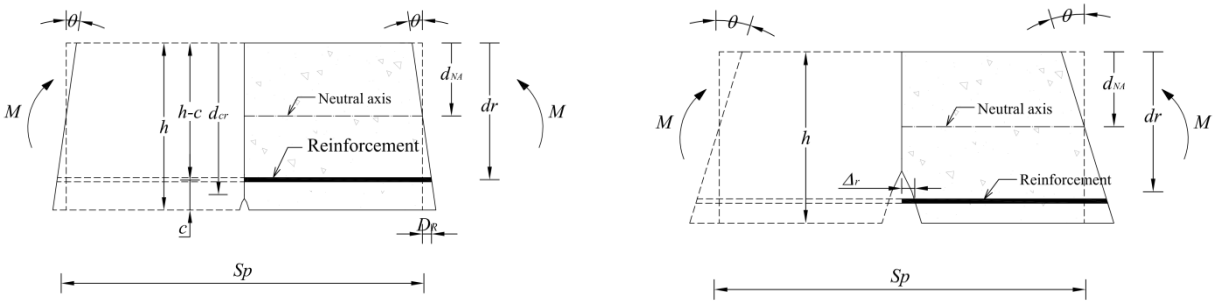

(a) (b)

Fig. 11: Deformation of reinforcement in flexural concrete member; (a) crack level is lower than reinforcement, (b) crack crossed the reinforcement

Therefore longitudinal deformation of the reinforcement (D_r) is equal to deformation of concrete and can be obtained from:

$$D_r = \theta(d_r - d_{NA}) \tag{66}$$

The tensile strain and corresponding stress of the reinforcement are determined from the following equations:

$$\varepsilon_{rt,i} = 2D_r / S_p \tag{67}$$

$$\sigma_{rt,i} = \sigma_{rt}(\varepsilon_{rt,i}) \quad (\text{for } d_i < d_{cr}) \tag{68}$$

Tensile force of the reinforcement is obtained from Eq. 68

$$F_{rt,i} = A_r \sigma_{rt,i} \qquad (\text{for } d_i < d_{cr}) \tag{69}$$

When reinforcement being crossed by crack $(d_r \geq d_{cr})$, collaboration of reinforcement in load carrying procedure is taken place depending on bond-slip and tension stiffening responses explained earlier. In this case, as depicted in Fig. 11b, crack widening at the level of reinforcement (Δ_r) is determined from Eq. (70):

$$\Delta_r = \frac{w_r}{2} \tag{70}$$

As represented in Eq. 37, slip at crack initiation $\left(\delta\left(x=0\right)\right)$ equals Δ_r. Therefore for the considered ascending bond-slip response, substituting Eq. 55, 62, or 64 in Eq. 46, tensile force of reinforcement at cracked section is determined corresponding to formation of primary, secondary and tertiary crack, respectively, as represented in Eq. 71:

$$F_{rt} = \begin{cases} \dfrac{(\Delta_r \lambda_1 E_c + 0.96\sigma_{ct}(w_r))A_r E_r}{0.96E_c} & \left(\sigma_{cr} E_r A_r / E_c\right) < F_{rt} \le F_{rt,cr}^{pr} \\ \dfrac{(\Delta_r \lambda_1 E_c + 0.76\sigma_{ct}(w_r))A_r E_r}{0.76E_c} & F_{rt,cr}^{pr} < F_{rt} \le F_{rt,cr}^{\sec} \\ \dfrac{(\Delta_r \lambda_1 E_c + 0.46\sigma_{ct}(w_r))A_r E_r}{0.46E_c} & F_{rt,cr}^{\sec} < F_{rt} \le F_{rt,cr}^{tri} \end{cases} \tag{71}$$

6 ALGORITHM TO PREDICT THE MOMENT–ROTATION RESPONSE OF FLEXURAL FRC ELEMENT WITH TENSILE LONGITUDINAL REINFORCEMENT

Deformation of a reinforced concrete prism subjected to the rotation of θ is depicted in Fig. 12. A cross section of Fig. 13a is considered, in general, for the beam, where the tensile reinforcements are positioned at the depth of d_r with respect to the compressive fibre of section. Cross section of the beam is then discretized into n layers as depicted in Fig. 13b, where the width and the thickness of ith layer located at the depth of d_i is designated, respectively, by b_i and t_i. For the layer positioned at the level of reinforcement $\left(d_i = d_r\right)$ the total width of layer $\left(b_i\right)$ divided to b_r and $b_c\left(=b_i - b_r\right)$, being effective width of reinforcement and its surrounding concrete, respectively, where b_r is obtained from the following equation:

$$b_r = A_r / t_i \tag{72}$$

where A_r is reinforcement area.

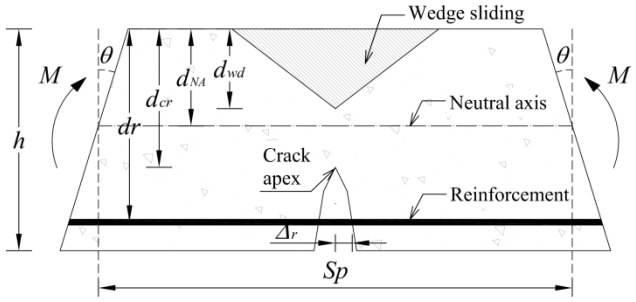

Fig. 12: Flexural deformation of a cracked prism of reinforced FRC

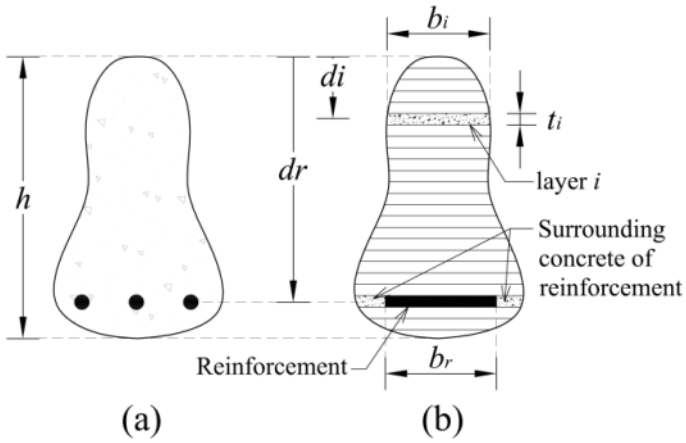

Fig. 13: (a) cross section of reinforced-FRC prism; (b) layering the cross section

It is assumed that material property of concrete in tension ($\sigma_{ct}(\varepsilon_{ct})$ and $\sigma_{ct}(w)$), and in compression ($\sigma_{cc}(\varepsilon_{cc})$), the tensile stress-strain relationship of reinforcement ($\sigma_{rt}(\varepsilon_{rt})$), and the bond-slip behaviour of reinforcement and concrete interface ($\tau(\delta)$) has been already obtained from material standard tests. To develop the aimed model a successive increment is imposed to the rotation of the prism (θ) of Fig. 12 and corresponding bending moment (M) is resulted in an iterative algorithm explained in the following:

1. Considering an increment of rotation of $\Delta\theta$, the imposed rotation corresponding to the *kth* step is obtained from Eq. (73):

$$\theta_k = k\Delta\theta \quad (k = 1 \rightarrow k_u) \tag{73}$$

2. An imaginary value is assumed for d_{NA}, depth of neutral axis in Fig. 12.

2.1 increment of i from 1 to n

2.2.1 Deformation of discrete layers is obtained:

$$D_i = \theta_k \left| d_i - d_{NA} \right| \tag{74}$$

2.2.2 For layers with $d_i < d_{NA}$: *(compressive region)*

$$\varepsilon_{cc,i} = 2D_i \ / S_p \tag{75}$$

2.2.2.1 If $\varepsilon_{cc,i} \le \varepsilon_{cc,pk}$ layer i is located outside the wedge area

$$F_{cc,i} = \sigma_{cc}\left(\varepsilon_{cc,i}\right) b_i t_i \tag{76}$$

2.2.2.2 If $\varepsilon_{cc,i} > \varepsilon_{cc,pk}$ layer i is located inside the wedge area: for which compressive strain of ε_i' is guessed:

$$S_i' = D_i - \varepsilon_i' S_p / 2 \tag{77}$$

$$H_i' = \frac{S_i'}{\cos\alpha} \tag{78}$$

Determining compressive force $\left(F_{cc,i}\right)$ from Eqs. 6 to 10.

Determining compressive stress of the layer corresponding to the imaginary value of ε_i'

$$\sigma_{cc,i}' = \frac{F_{cc,i}}{b_i t_i} \tag{79}$$

Determining compressive strain $\left(\varepsilon_{cc,i}'\right)$ of the layer corresponding to the imaginary value of ε_i' by substituting $\sigma_{cc,i}'$ into Eq. 1.

If $\left|\varepsilon_{cc,i}' - \varepsilon_i'\right| \le Tol.$ keeping $F_{cc,i}$, otherwise jumping back to step 2.2.2.2 with new value of ε_i'

2.2.3 For layers with $d_i \ge d_{NA}$: *(tensile region without reinforcement)*

$$\varepsilon_{cc,i} = 2D_i / S_p < \varepsilon_{cr} \tag{80}$$

2.2.3.1 If $\varepsilon_{ct,i} \le \varepsilon_{cr}$ layer i is located outside the cracked region:

$$F_{ct,i} = \sigma_{ct}\left(\varepsilon_{ct,i}\right) b_i t_i \tag{81}$$

When $\varepsilon_{ct,i} = \varepsilon_{cr}$ keeping d_i as d_{cr} .

2.2.3.3 If $\varepsilon_{ct,i} > \varepsilon_{cr}$ layer i is located inside the cracked region:

$$w_i = \left[2D_i - \frac{\sigma_{ct}\left(w_i\right)}{E_c} S_p \right] \tag{82}$$

$$F_{ct,i} = \sigma_{ct}\left(w_i\right) b_i t_i \tag{83}$$

2.2.4 For layer with $d_i = d_r$: *(tensile reinforcement)*

2.2.4.1 If $d_r \le d_{cr}$:

$$\varepsilon_{rt,i} = 2D_i / S_p \tag{84}$$

$$F_{rt,i} = b_i t_i \sigma_{rt}\left(\varepsilon_{rt,i}\right) \tag{85}$$

2.2.4.2 If $d_r > d_{cr}$:

$$\Delta_r = \frac{w_r}{2} \tag{86}$$

$$F_{rt} = \begin{cases} \dfrac{(\Delta_r \lambda_1 E_c + 0.96\sigma_{ct}(w_r))A_r E_r}{0.96E_c} & \left(\sigma_{cr} E_r A_r / E_c\right) < F_{rt} \le F_{rt,cr}^{pr} \\ \dfrac{(\Delta_r \lambda_1 E_c + 0.76\sigma_{ct}(w_r))A_r E_r}{0.76E_c} & F_{rt,cr}^{pr} < F_{rt} \le F_{rt,cr}^{\sec} \\ \dfrac{(\Delta_r \lambda_1 E_c + 0.46\sigma_{ct}(w_r))A_r E_r}{0.46E_c} & F_{rt,cr}^{\sec} < F_{rt} \le F_{rt,cr}^{tri} \end{cases} \tag{87}$$

2.2.5 Assessment of force equilibrium:

If $\left|\sum F_{ct,i}^k + F_{rt}^k - \sum F_{cc,i}^k\right| \le Tol.$, the considered value of d_{NA} is correct, otherwise jump to step 2 assuming a new value of d_{NA} .

3. Determining the bending moment of section:

$$M_k = \sum d_i F_{cc,i}^k + \sum d_i F_{ct,i}^k + d_r F_{rt}^k \tag{88}$$

4. Saving (θ_k, M_k)

7 MODEL TO ESTIMATE THE FORCE-DEFLECTION RELATIONSHIP

To evaluate the force-deflection response of a statically determinate RC beam (or a slab's strip), the structural element is decomposed in m segments of length Δx. The moment-rotation relationship for each segment Δx representative of the beam (in terms of cross section geometry, materials and flexural reinforcement) is determined, and then converted in a moment-curvature relationship according to Eq. (89), since curvature is not dependent of the length of the adopted segments:

$$\chi_k = \frac{\varepsilon_{cc,1}}{d_{NA}} \tag{89}$$

being $\varepsilon_{cc,1}$ the concrete compressive strain at the top surface of the cross section. According to this approach, for successive χ_i of the $M-\chi$ relationship of the beam mid-span section the corresponding M_i is read, and the total applied load P_i is determined by equilibrium of the beam, as well as the beam bending diagram M_i. Decomposing the beam in small segments, the bending moment in a generic cross section at a distance x can be determined, $M_i(x)$, and from the $M-\chi$ relationship of this cross section, the corresponding flexural stiffness $EI_i(x)$ is obtained, as well as the bending moment in this section for the base system corresponding to the evaluation of the deflection at the beam mid-span, $\bar{M}(x)$. By applying the Virtual Work Method, the mid-span deflection of the beam for the ith loading step, $(\delta_{mid})_i$, is determined, which, together with P_i provides a point of the P-δ curve.

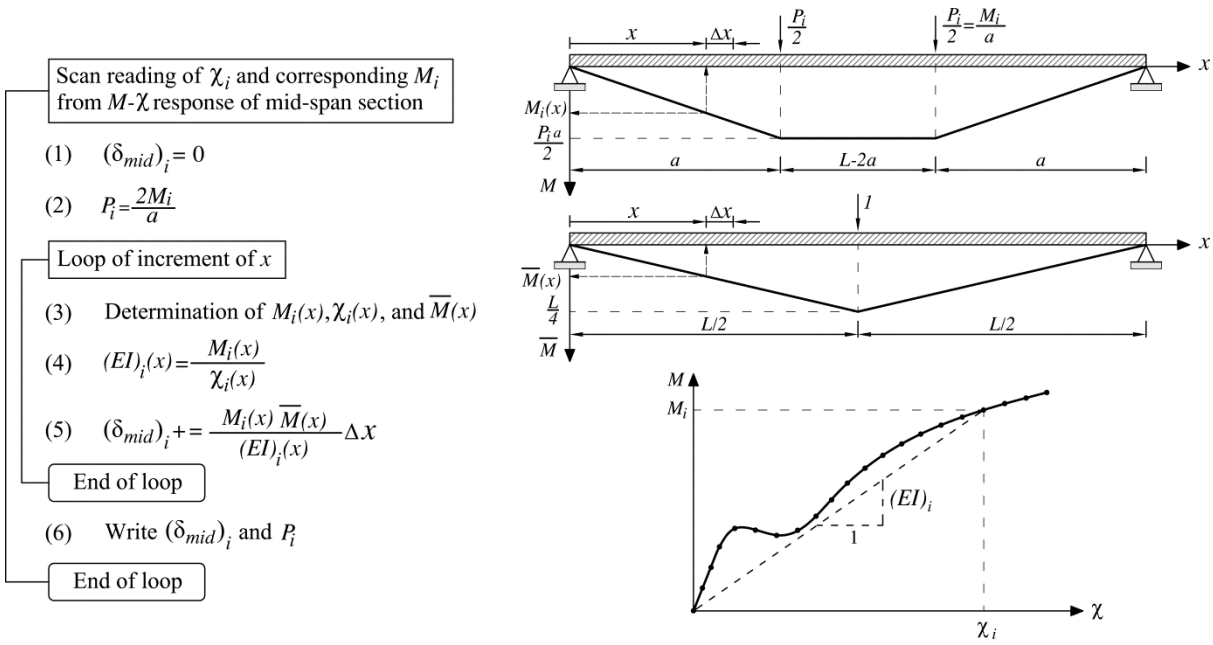

Fig. 14: Numerical approach to simulate the force-deflection response of simple supported beams

8 MODEL APPRAISAL

The performance of the proposed model in terms of predicting the force-deflection response is evaluated by simulating the force-deflection relationship in R/FRC beams tested by Barros *et al.* [34]. The parameterized geometry and reinforcement arrangement of the beams of the three simulated experimental programs are represented in Fig. 15, and the corresponding data is indicated in Table 1. In these three experimental programs SFRC was used, and a four point loading configuration was adopted.

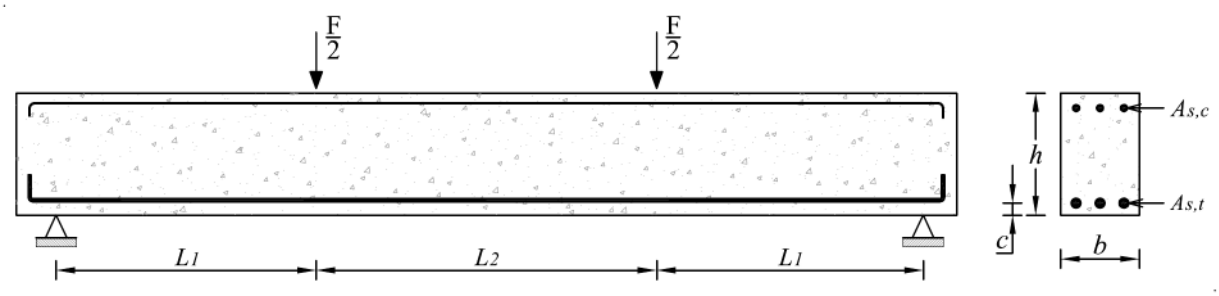

Fig. 15: Reinforced SFRC beam under four point loading configuration (data included in Table 1).

Table 1: Geometric properties of the beams (Fig. 15)

Beam series	Reference	b [mm]	h [mm]	c [mm]	L_1 [mm]	L_2 [mm]	$A_{s,t}$ [mm^2]	$A_{s,c}$ [mm^2]
B1							84.8	
B2	Barros *et al.* [30]	350	150	20	450	450	150.8	84.8
B3							235.6	

The B1, B2, and B3 beams were made by a concrete reinforced with 45 kg/m^3 of hooked ends steel fibers of a length and diameter of 60 and 0.75 mm, respectively. The concrete compressive strength and the yield stress of the longitudinal steel bars are the relevant available information. To derive the constitutive law for defining the tensile behavior of SFRC, an inverse analysis procedure was executed by matching, as much as possible, the force-deflection response registered experimentally in the B1 beam. The obtained data is included in Table 2. The Young's modulus was determined from Eq. (90) for SFRC utilized in B1-B3 for both in tension and in compression. For the k_e bond stiffness the value 70 MPa/mm was used.

$$E_c = 21.5\left(\frac{f_{cc}}{10}\right)^{1/3} \ (GPa) \tag{90}$$

In Fig. 16 the force-deflection response of B1, B2 and B3 beams, obtained by the developed numerical strategy, is compared to the corresponding one registered experimentally, being evident the good predictive performance of the model.

Table 2: Mechanical properties of intervening materials of the simulated beams

Beam series	f_{cc} [MPa]	f_{ct} [MPa]	α_1 -	α_2 -	α_3 -	α_4 -	α_5 -	w_1 [mm]	w_2 [mm]	w_3 [mm]	w_4 [mm]	w_5 [mm]	w_u [mm]	f_{sy} [MPa]	ε_{su} [‰]
B1														600	10
B2	99.2	2.53	0.86	0.83	0.64	0.36	0.27	0.01	0.1	0.3	0.6	1.8	3.0	670	15
B3														680	12

E_s = 200 GPa

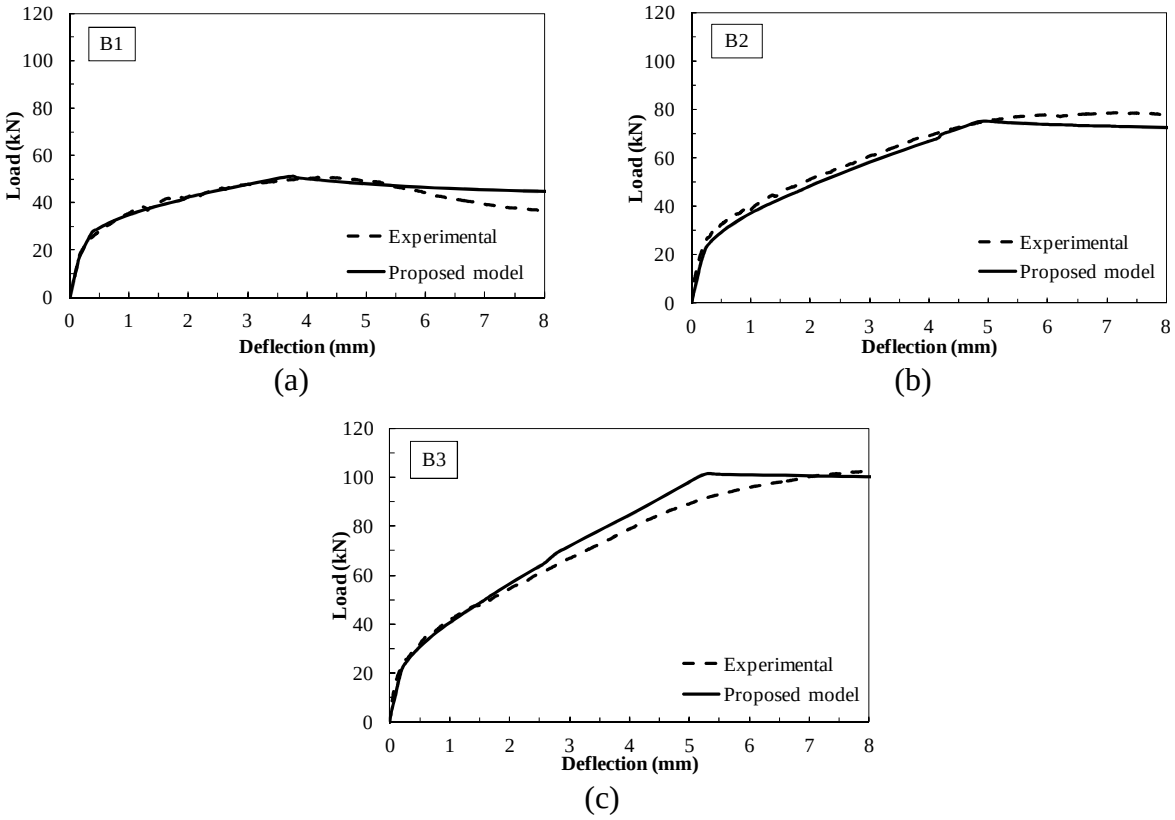

Fig. 16: Load-deflection response predicted by the proposed model and recorded in the experimental program.

The influence of the magnitude of Δx on the force-deflection responses was evaluated by adopting different values of Δx to determined the force-deflection relationship of B1 beam whose result is represented in Fig. 17. Fig. 17 reveals that the magnitude of Δx adopted in the algorithm of Fig. 14 has no effect on the accuracy of the force-deflection response of the beam.

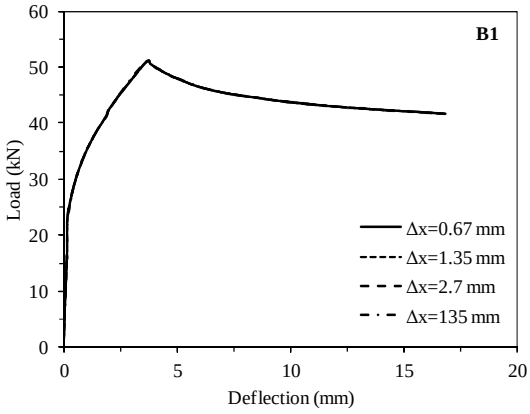

Fig. 17: Influence of the magnitude of Δx on the force-deflection response of B1beam determined from the algorithm of Fig. 14.

9 IMPACT OF SHRINKAGE ON MOMENT-ROTATION BEHAVIOR

When concrete is subjected to a sustained load, time dependent strain due to shrinkage develops. This shrinkage strain has considerable impact on the performance of structural members, causing increased crack widths and deflections which may result in serviceability failure. Time effects on reinforced concrete has been an area of research interest for more than 80 years, with much effort devoted to the development of models to predict changes in concrete material behaviour with time [35,36]. These approaches utilize methods of varying complexity to determine the change in concrete material properties with time and, hence, cross sectional behaviour. However in mechanics terms, all of these approaches are based on a moment-curvature (M/χ) analysis technique: in which there is a linear strain profile; and in which there is full interaction, that is, the reinforcement does not slip relative to the concrete so that there is a uni-linear strain profile. These assumptions mean that the techniques are unable to describe crack spacing or widening directly and, therefore, must resort to empirically derived approaches to do so. In the following the M/θ approach is extended to account the influence of shrinkage in order to prediction load-carrying capacity of reinforced FRC members.

According to Eurocode2 [37] recommendation the total shrinkage strain (ε_{cs}) is composed of two components, the drying shrinkage strain (ε_{cd}) and the autogenous shrinkage strain (ε_{ca}):

$$\varepsilon_{cs} = \varepsilon_{cd} + \varepsilon_{ca} \tag{91}$$

The drying shrinkage strain develops slowly, since it is a function of the migration of the water through the hardened concrete. The development of the drying shrinkage strain in time follows from:

$$\varepsilon_{cd}(t) = \beta_{ds}(t - t_s).k_h.\varepsilon_{cd,0} \tag{92}$$

where k_h is a coefficient depending on the notional size of the cross-section, $h_0 = 2A_c/u$, where A_c is the concrete cross-sectional area and u is the perimeter of that part which is exposed to drying. k_h parameter is obtained from Table 3. $\varepsilon_{cd,0}$ is dependent of strength class of concrete and humidity of environment can be obtained from Table 4.

Table 3: Values for k_h

h_0	k_h
100	1.0
200	0.85
300	0.75
≥ 500	0.7

Table 4: Nominal unrestrained drying shrinkage values $\varepsilon_{cd,0}$ (in 0/00) for concrete

f_{ck} / $f_{ck,cube}$ (MPa)	Final unrestrained drying shrinkage (in 0/00) Relative Humidity (in 0/0)					
	20	40	60	80	90	100
20/25	0.64	0.60	0.50	0.31	0.17	0
40/50	0.51	0.48	0.40	0.25	0.14	0
60/75	0.41	0.38	0.32	0.20	0.11	0
80/95	0.33	0.31	0.26	0.16	0.09	0
90/105	0.30	0.28	0.23	0.15	0.05	0

.

$\beta_{ds}(t-t_s)$ in Eq. 92 is determined from following equation:

$$\beta_{ds}(t-t_s)=\frac{(t-t_s)}{(t-t_s)+0.04\sqrt{h_0^3(mm)}} \tag{93}$$

where t is the age of the concrete at the moment considered in days, t_s is the age of the concrete (days) at the beginning of drying shrinkage, normally this is at the end of curing.

The autogenous shrinkage strain develops during hardening of the concrete: the major part therefore develops in the early days after casting. Autogenous shrinkage is a linear function of the concrete strength can be obtained as following:

$$\varepsilon_{ca}(t)=\beta_{as}(t).\varepsilon_{ca,\infty} \tag{94}$$

where:

$$\varepsilon_{ca,\infty}=-2.5(f_{ck}-10)\times 10^{-6} \tag{95}$$

and

$$\beta_{as}(t)=1-\exp(0.2t^{0.5}) \tag{96}$$

t in the above equation is time in days.

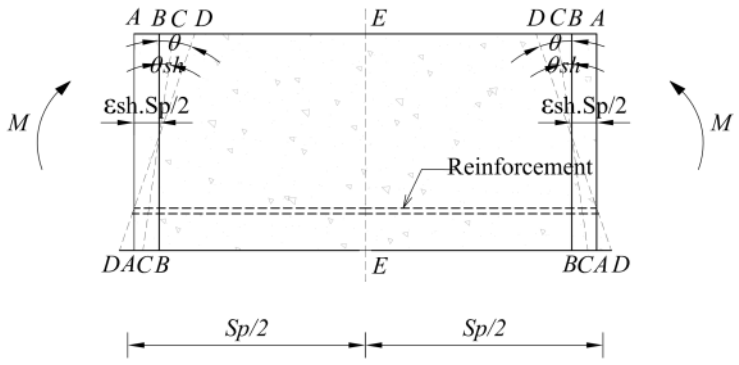

Fig.18: Segmental M/θ

Impact of shrinkage in the *M/θ* mechanism is schematized in Fig. 18 for a segment of a beam (A-A-A-A) of length S_p . Prior to any deformations taking place, either as a result of shrinkage or the application of an external load, both the concrete and the reinforcement are of the length S_p. If a shrinkage strain ε_{sh} take place and the concrete be free of any restraint from the reinforcement, a deformation equal to $\varepsilon_{sh} S_p / 2$, would take place from A-A to B-B over each half of the segment A-E. However, due to the presence of reinforcement, the concrete is restrained and, hence, the actual deformation of the concrete will be from A-A to C-C that causes a shrinkage rotation designated by θ_{sh}. If a constant moment *M* be applied over the segment, a further rotation takes place and finally the total rotation will be equal to θ and the deformation from B-B equal to D-D.

For the case shrinkage strain is lower than cracking strain of concrete, a full interaction between concrete and reinforcement can be assumed. In this case an initial curvature due to shrinkage will be formed in the prism before applying the load (Fig. 19).

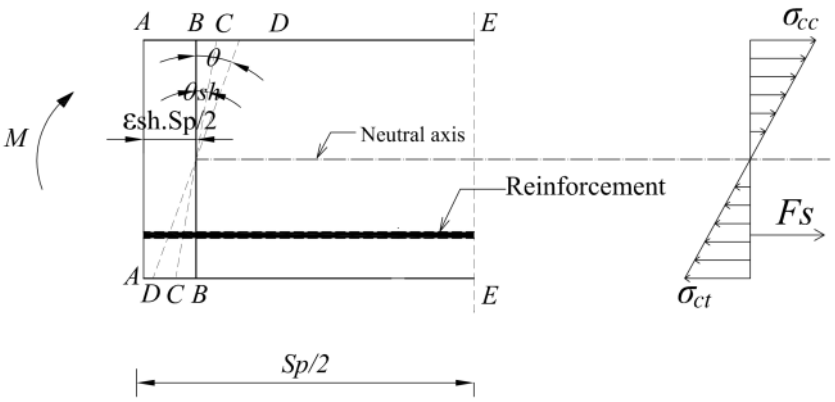

Fig.19: Analysis of an uncracked segment.

In Fig. 19, since any deformation from A-A causes a stress in the reinforcement, A-A becomes the baseline to measure deformation of reinforcement in order to induce internal stress of reinforcement. Similarly if the concrete was free to shrink without restraint, then it would reduce in length $\varepsilon_{sh} S_p / 2$ from A-A to B-B. This shortening would not induce a stress in concrete. Hence any deformation of the concrete away from B-B induces a stress in the concrete and, therefore, B-B becomes the baseline for concrete deformations according which stress of concrete should be measured. Considering these two baselines strain and stress for each layer of concrete and also strain and stress of reinforcement can be obtained and used to determine the internal force of section.

Noticeable point is that shrinkage deformation of the prism would not disturb equilibrium of internal force and bending moment though the section, Hence for the case strain shrinkage is the sole strain imposed to the section, satisfying the equilibrium of force and moment of section in an iterative calculation, the shrinkage rotation of θ_{sh} and correspondingly the depth of neutral axes will be obtained. θ_{sh} is the initial rotation imposed to the prism just before loading.

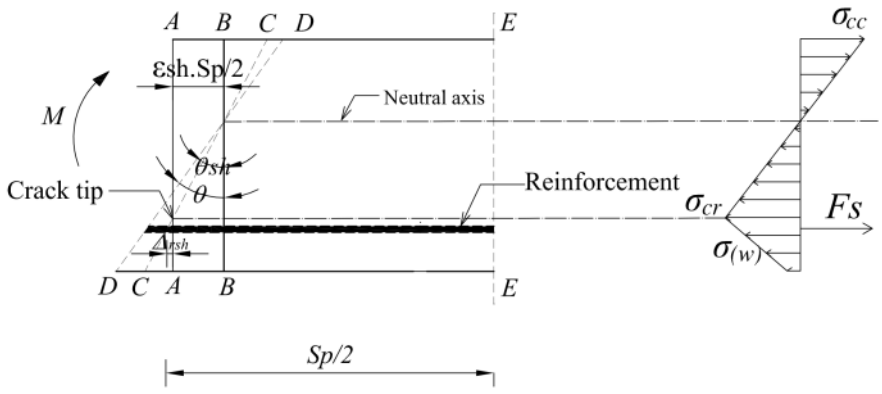

Fig.20: Cracked segment analysis

In Fig. 20 is depicted internal deformation and stress distribution of the case the shrinkage strain (in layer of reinforcement) larger than cracking is imposed to the prism, according which crack apex is above the reinforcing bar. In this case the partial interaction must be used to describe the behaviour of the tensile reinforcement. In this case the load developed in the reinforcement is dependent on the slip of the bar at the crack face. Δ_{rsh} in Fig. 20 depends on the bond slip (τ / δ) properties between the bar and the concrete surrounding it.

The impact of shrinkage on moment-rotation responses was evaluated in a reinforced FRC prism with rectangular cross section. Height and width of the section was 300 mm and 150 mm, respectively. A steel bar with a diameter of 12 mm was considered as reinforcement placed at 50 mm depth from bottom tensile face of the section. The tensile properties of the steel are indicated in Table 3.

Table 5: Values of the main properties of steel bar

Diameter (mm)	Yield strain (ε_{sy})(‰)	Yield stress (σ_{sy}) (MPa)	Maximum strain (ε_{su}) (‰)	Modulus of elasticity(Es) (GPa)
12	3.0	585	14.3	200

The constitutive law considered for FRC is depicted in Fig. 21. A good bond condition was assigned to reinforcement and surrounding concrete interface. Therefore, assuming concrete compressive strength of $f_{cm} = 68$ MPa, the maximum bond was obtained equal to $2.5\sqrt{f_{cm}}$ =20.61 MPa.

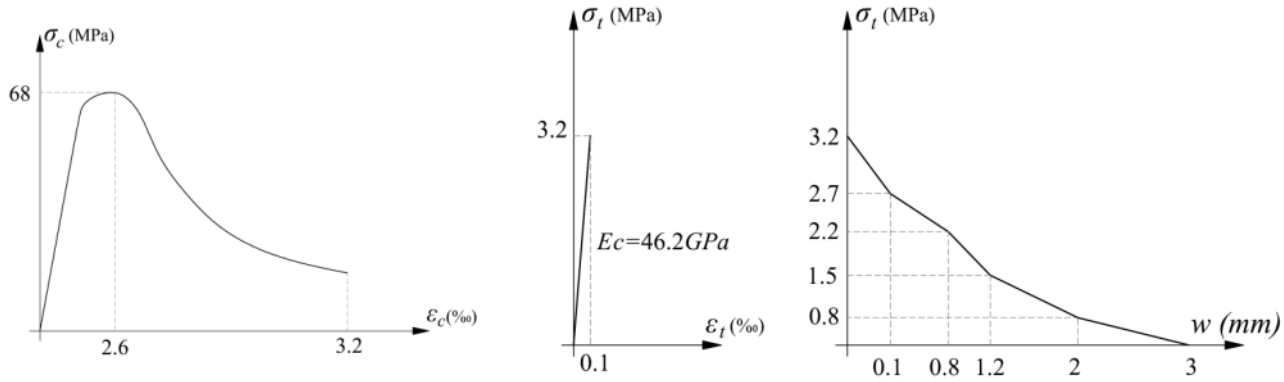

(a) (b)

Fig. 21: FRC constitutive laws; a) in compression, b) in tension

Regarding to the considered strength class of FRC and recommendation of Eurocode represented in Tables 3 and 4, the total shrinkage strain of 0.391, 0.97, 2.01 ‰ were obtained for 28, 90 and 180 days, respectively, for the assumed relative humidity of 40 %.

In Fig. 22 and 23, are compared, respectively, the impact of shrinkage on moment-rotation and moment-crack width of the prism. According to Fig. 22, resisting bending moment of the prism decreased 11 and 18%, respectively for 90 and 180 days, when compared to bending capacity of prism at 28 day. However the decreasing of resisting bending moment of the prism among 90 and 180 days was 8%, indicates detraction of impact of shrinkage.

According to Fig. 23, crack widening of the prism corresponding to resisting bending moment, was 0.62, 0.68, and 0.69, respectively for 28, 90, and 180 days. This means that taking in to account the concept of shrinkage increase 10, and 11% of crack width at 90 and 180 days when compared to 28 day.

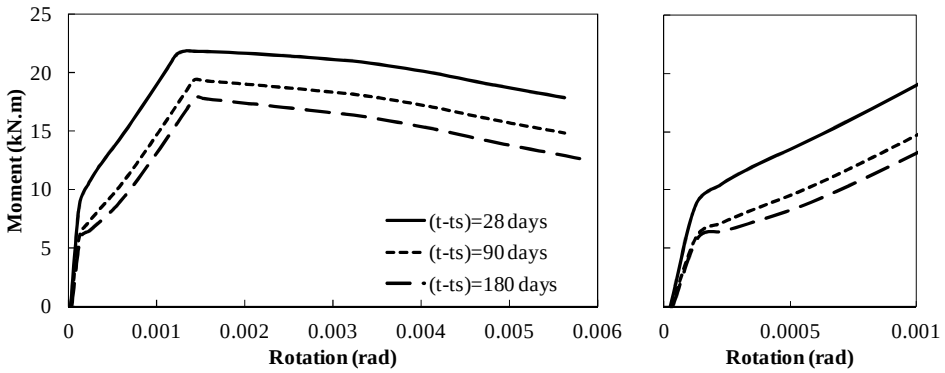

Fig. 22: Effect of shrinkage on moment-rotation response of the sample beam.

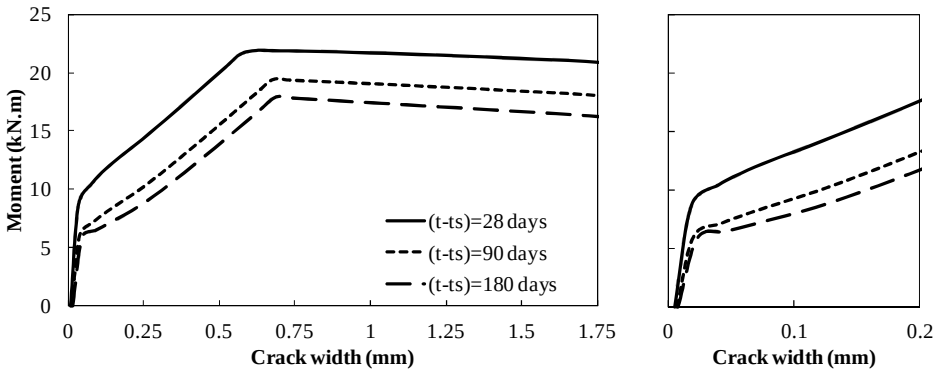

Fig. 23: Effect of shrinkage on moment-crack width response of the sample beam.

10 CONCLUSION

In the present report, taking advantage of concept of moment-rotation $(M-\theta)$ an analytical model was developed to determine the load carrying capacity of flexural FRC elements strengthened by tensile longitudinal reinforcement. The model is capable to consider the bond characteristics of reinforcement and surrounding concrete, stress-crack width constitutive law of fibrous concrete, and also the shear friction mechanism of concrete in compression as the reason of softening post-peak deterioration in compressive stress-strain response of concrete. Adopting recommendation of Eurocode, concept of shrinkage was imposed to the model, which gives to the model capability of taking into account time dependent deterioration of the load-carrying capacity and the durability contexts of the reinforced concrete.

11 REFERENCES

[1] Naaman, A.E., Reinhardt, H., "Proposed classification of HPFRC composites based on their tensile response", Materials and Structures, 39, 547-555, (2006).

[2] Taheri, M., Barros, J.A.O., Salehian, H., "A design model for strain-softening and strain-hardening fiber reinforced elements reinforced longitudinally with steel and FRP bars", Journal of Composites, Part B engineering, 42, 1630–1640, (2011).

[3] Taheri, M., Barros, J.A.O., Salehian, H., "A parametric study on the use of strain softening/hardening FRC for RC elements failing in bending", ASCE Materials in Civil Engineering Journal, 24 (3), 259-274, (2012).

[4] Barros, J.A.O., Taheri, M., Salehian, H., Mendes, P. J.D., "A Design Model For Fibre Reinforced Concrete Beams Pre-Stressed With Steel and FRP Bars", Composite Structures Journal, 94 (8), 2494-2512, (2012).

[5] Haskett, M., Oehlers, D.J., Visintin, P., Ali Mohamed, M.S., "Using shear-friction properties to simulate concrete softening in reinforced concrete flexural members" Submitted to: Cement and Concrete Research, (2012).

[6] Hognestad, E., Hanson, N.W., McHenry, D., "Concrete stress distribution in ultimate strength design", Journal of ACI, 27 (4), 455-479,(1955).

[7] Tasdemir, M.A., Tasdemir, C., Akyuz, S., Jefferson, A.D., Lydon, F.D., Barr, B.I.G., "Evaluation of Strains at Peak Stresses in Concrete: A Three-Phase Composite Model Approach", Cement and Concrete Composites, 20 (4), 301-318,(1998).

[8] Haskett M., Oehlers D.J., Mohamed Ali M.S., Sharma, S.K., "The shear-friction aggregate-interlock resistance across sliding planes in concrete", Magazine of Concrete Research, Vol. 62, No. 12, 907-924, (2010).

[9] Haskett M., Oehlers D.J., Mohamed Ali M.S., Sharma, S.K., "Evaluating the shear-friction resistance across sliding planes in concrete", Engineering Structures, Vol 33, No. 4, 1357-1364, (2011).

[10] Haskett M, Oehlers DJ, Visintin P., and Mohamed Ali, MS. "Using shear-friction to simulate concrete softening in RC flexural members", submitted to Cement and Concrete Research 2011.

[11] Visintin, P., "A generic segmental analysis of all types of RC members", PhD thesis, University of Adelaide, (2012).

[12] Oehlers, D.J., Mohamed Ali M.S., Haskett, M., Lucas, W., Muhamad, R., Visintin, P., "FRP reinforced concrete beams – a unified approach based on IC theory", ASCE Composites for Construction, May/June, Vol. 15, No. 3, pp293-303, (2011).

[13] Barros, J.A.O., Pereira, E.B., Santos, S.P.F.,"Lightweight panels of steel fiber reinforced self-compacting concrete", Journal of Materials in Civil Engineering, 19(4), 295-304, (2007).

[14] Barros, J.A.O., "Steel fiber reinforced self-compacting concrete – from the material characterization to the structural analysis", HAC2008, 1st Spanish Congress on Self-Compacting Concrete, Valencia, Spain, 31-58, 18-19 February, (2008). (Invited Keynote Lecturer).

[15] Formagini, S., Fairbairn, E.M.R., Toledo Filho, R.D.,"Mix Design and Characterization of Ultra High Performance Fiber Reinforced Cement Composites", IBRACON journal, 3(1), 1-14, (2007).

[16] Naaman, A., "High performance fibre reinfoced cement composites" In C. Shi, & Y. Mo, "High-performance construction materials (Science and Application)", World Scientific Publishing Co. Pte. Ltd, (2008).

[17] Cunha, V.M.C.F.,"Steel Fibre Reinforced Self-Compacting Concrete – from Micromechanics to Composite behaviour", PhD Thesis, University of Minho, (2009).

[18] Harajli, M.H., "Effect of confinement using steel, FRC, or FRP on the bond stress-slip response of steel bars under cyclic loading", Materials and Structures, 39,621–634, (2006).

[19] Hamad, B. S., Harajli, M. H., and Jumaa, G. "Effect of fiber reinforcement on bond strength of tension-lap splices in high strength concrete", ACI Material journal, 98 (5), 638–647, (2001).

[20] Harajli, M., Hamad, B., Karam, K., "Bond-slip Response of Reinforcing Bars Embedded in Plain and Fiber Concrete", Journal of Materials in Civil Engineering, Vol. 14, No. 6, December 1, (2002).

[21] Campione, G., Cucchiara, C., Lamendola, L., Papia, M., "Experimental investigation on local bond-slip behaviour in lightweight fiber reinforced concrete under cyclic actions", 13th World Conference on Earthquake Engineering Vancouver, B.C., Canada, No. 2087, 1-6, August, (2004).

[22] Ehsani, M.R., Saadatmanesh, H., Tao, S., "Bond Behavior of Deformed GFRP Rebars" Journal of Composite Materials, Vol. 31, No. 14, pp1413-1430, (1997).

[23] Abdalla, H.A., "Evaluation of Deflection in Concrete Members Reinforced with Fibre Reinforced Polymer (FRP) Bars", Composite Structures, 56, 63-71, (2002).

[24] Masmoudi, R., Theriault, M., Benmokrane, B., "Flexural behaviour of concrete beams reinforced with deformed fiber reinforced plastic reinforcing rods", ACI Struct J, 95(6),665 –76, (1998).

[25] Aiello, M.A., Leone, M., Pecce, M., "Bond Performances of FRP Rebars-Reinforced Concrete", J. Mater. Civ. Eng, 19(3), 205-213, (2007).

[26] Achillides, Z., Pilakoutas, K., "Bond Behavior of Fiber Reinforced Polymer Bars under Direct Pullout Conditions", J. Compos Constr, 8(2), 173-181, (2004).

[27] Almusallam, T.H., "Analytical prediction of flexural behavior of concrete beams reinforced by fiber reinforced polymer (FRP) bars", J Compos Mater, 31(7), 640–57, (1997).

[28] Pecce, M., Manfredi, G., Cosenza, E., "Experimental response and code models of GFRP RC beams in bending", J Compos Constr, 4(4),182–90, (2000).

[29] Rossetti, V.A., Local bond stress-slip relationships of glass fiber reinforced plastic bars embedded in concrete", Materials and Structures, 28, 340-344, (1995).

[30] Model Code 2010, Final draft, CEB-FIP, (2011).

[31] Mazaheripour, H., Barros, J., Soltanzadeh, F., Gonçalves, D., "Interfacial bond behaviour of GFRP bar in self-compacting Fiber Reinforced Concrete", BEFIB conference,fiber reinforced concrete, (2012).

[32] Tighiouart, B., Benmokraneu, B., Gao, D., "Investigation of bond in concrete member with fiber reinforced polymer (FRP) bars", Construction and Building Materials, 12, 453-462, (1998).

[33] Belarbi, A., Wang, H., "Bond-Slip Response of FRP Reinforcing Bars in Fiber Reinforced Concrete under Direct Pullout", Concrete, (2004).

[34] Barros JAO, Santos SPF, Lourenço LAP, Gonçalves DMF. Flexural behaviour of steel fibre reinforced self-compacting concrete laminar structures. In: Barragán B, Pacios A, Serna P, editors. 1st Spanish Congress on Self-Compacting Concrete (HAC2008). Valencia2008. p. 567-78.

[35] Neville, A.M., Dilger, W.H. and Brooks, J.J. (1983) “Creep of Plane and Structural Concrete Structures”, Construction Press Longman Group Ltd.

[36] American Concrete Institute (ACI). (1982). “Prediction of creep, shrinkage and temperature effects in concrete structures.” ACI-209R-82, ACI Committee 209, Detroit.

[37] prEN 1992-1-1, “Eurocode 2: Design of concrete structures – Part 1: General rules and rules for buildings”, April (2002).